Textures and Microstructures, Vol. 33, pp. 93–110
Reprints available directly from the publisher
Photocopying permitted by license only

TEXTURE AND MAGNETIC LEVITATION FORCE OF MELT-TEXTURED YBaCuO CYLINDERS

V. JUNG[a,*], M. ADAM[a], H.J. BORNEMANN[a], H.-G. BROKMEIER[b], A. KAISER[a], R. SCHNIEBER[b] and J. THOMS[a]

[a]*Forschungszentrum Karlsruhe, Institut für Nukleare Festkörperphysik, P.O.B. 3640, D-76021 Karlsruhe, Germany;* [b]*TU Clausthal/GKSS Geesthacht, P.O.B. 1160, D-21494 Geesthacht, Germany*

To investigate the correlation between the levitation force of YBaCuO cylinders when approached by a permanent magnet and the texture of these YBaCuO cylinders some of these specimens were selected which are free of microcracks, have the same oxygen load, show no isotropic fraction or other undesired parasitic *c*-axis orientations. To gain a maximum levitation force the *c*-axis orientation of the crystalline domains has to have a small divergence between the *c*-axis and the cylinder axis. By measurements of the (002) pole figures by neutron diffraction with a mesh width no more than 6° undesired *c*-axis orientations have been analyzed. The distribution of the *c*-axis near the cylinder axis has been measured at the (005) reflection of 7 times higher intensity than the (002) reflection. The angular limit within which lie 94% of all *c*-axis orientations is a practical value for comparison of the *c*-axis orientations and the levitation forces of the different YBaCuO cylinders.

Keywords: Orientation and current carrying capacity; YBaCuO; Magnetic bearing

1 INTRODUCTION

Self-stabilizing superconducting magnetic bearings (Jung, 1988) require clearly textured solid cylinders of YBaCuO (Bornemann *et al.*, 1993a). The YBaCuO cylinders generated in a melt and highly textured by means of a seed crystal are subjected to measurement of their maximum

* Corresponding author.

levitation forces by a permanent magnet of 0.6 T moved close to the cylinders (Bornemann *et al.*, 1997). The respective maximum levitation force is reached whenever the inducing permanent magnet nearly contacts the cylindrical specimen. The hysteresis effect produced as the permanent magnet is moved either towards or away from the specimen is brought about by the shielding of the external field by the superconductor. The maximum levitation force determined in this way is a function of many parameters, including oxygen loading and stoichiometry, also of the presence of microcracks in the specimen which would divert the current and, in this way, greatly reduce the levitation force. Although microcracks are unimportant in textural studies, they do reduce the levitation force considerably; consequently, specimens with microcracks cannot be used for correlations between the texture and the levitation force. In specimens under the same oxygen load and with identical stoichiometries, all of them without microcracks, the maximum levitation force is a function solely of the quality of the texture (Schochlin *et al.*, 1995). This correlation between the levitation force and the texture is to be clarified in this study. All levitation forces were measured with the same permanent magnet of only 25 mm diameter, 18 mm smaller than most specimens to be measured, which were 43 mm in diameter (Bornemann *et al.*, 1995). This means that a less well developed texture at the fringes of the solid YBaCuO cylinder to be examined has a less pronounced impact reducing the levitation force. Moreover, smaller specimens of only 33 mm diameter indicate the same levitation force as those of 43 mm diameter, see Fig. 1.

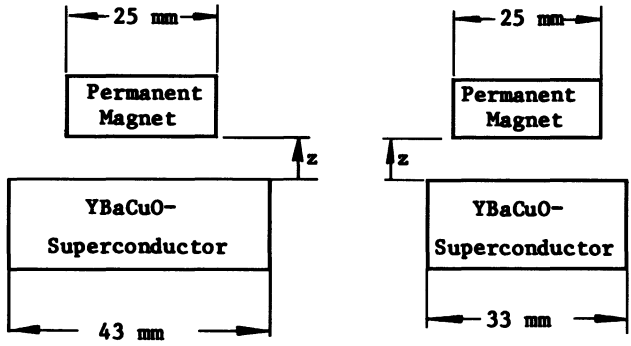

FIGURE 1 Geometry of permanent magnet and YBaCuO cylinder. A plot shows the levitation force as function of the levitation height. The hysteresis effect is produced by screening of the field.

2 ALIGNMENT OF *c*-AXES

The ideal alignment of the *c*-axes of the crystalline domains in the solid YBaCuO cylinder would be parallel to the axis of the cylinder and thus normal to the superconducting currents induced on concentric circles around the cylinder axis. However, this ideal case will never be achieved, unless in a single crystal. Single crystals, on the other hand, suffer from the draw-back of having no defects for flux pinning in a superconductor. A certain amount of disorder is necessary (Bogner, 1988).

Of course, theoretically, a texture can be designed so that all *c*-axes are normal to the direction of the induced current, but constitute different angles with the cylinder axis. In that case, the *c*-axes would have to be located in same planes with the cylinder axes. Again, this is an ideal case not likely to occur. However, what can occur is a mix of disorder and preferred direction. Thus, identical global textures of all specimens can have very different local textures. In this way, specimens with the same global texture can result in very different levitation forces. Figure 2 shows the various possible orientations of the *c*-axes relative to the cylinder axis. As can be seen in Fig. 3, the angle between the direction of the induced field, H, and the *c*-axis of a domain can assume values of up to $\pm 20°$ at an induction of 1 T without causing the current carrying

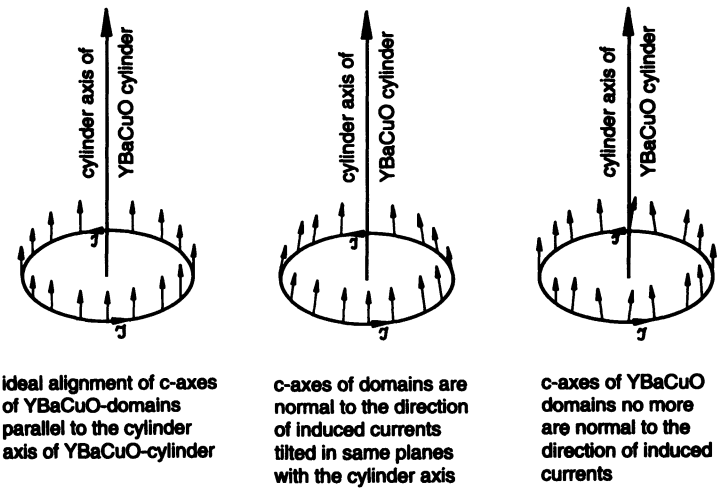

FIGURE 2 Different possibilities of alignment of the *c*-axes of YBaCuO domains.

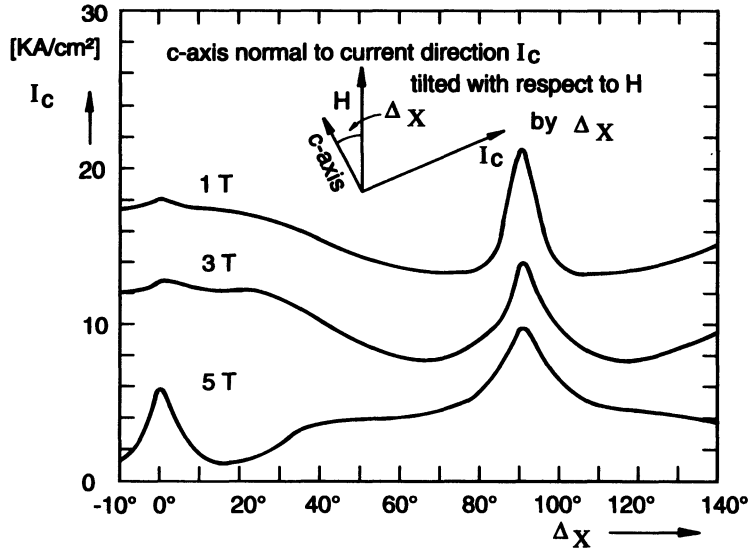

FIGURE 3 Dependence of current carrying capacity on the angle between field vector H and c-axis with field strength as parameter.

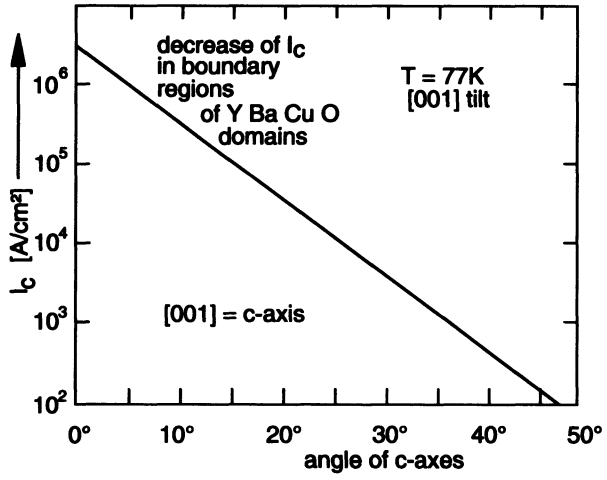

FIGURE 4 Decrease of J_c in boundary regions of YBaCuO domains in dependence on the tilting angle between domains.

capacity of the superconductor to suffer greatly. Only at fields of 5 T, this angle between the field vector and the *c*-axis must not exceed $\pm 1°$ (Bornemann *et al.*, 1993b). These relationships are shown in Fig. 3. At any rate, a critical factor is tilting of the *c*-axes of adjacent domains. A mere tilting angle of 10° reduces the maximum current carrying capacity of the boundary region between domains tilted relative to each other to one-tenth the level at 0° tilting, see Fig. 4 (Gross, 1993).

3 POLE FIGURE MEASUREMENT WITH NEUTRON DIFFRACTION

To find out whether a specimen is fully textured (i.e. has no random fraction) and contains no parasitic undesired texture, the entire pole figure must be scanned in a long equal-area measurement with a mesh width not exceeding 6° at the (002) reflection (Brokmeier, 1995; Bornemann *et al.*, 1996). Determining the isotropic fraction would take very long measurement times, for (1), the intensity of the (002) reflection is approximately one-seventh that of the (005) reflection, and the (2) the maximum counting rate at the peak of an orientation distribution is up to a factor 1000 higher than in a case in which the same intensity would be uniformly distributed over the entire pole sphere. A random fraction is much more easily determined from a comparison of the integral reflectivities of the orientation distributions of various specimens, as will be shown later in a comparison of the integral reflectivities of the M37 and M43 specimens. The orientation distributions of the *c*-axes of the specimens then, after rough measurement of all pole figures at the (002) reflection with a coarse mesh width, can be measured at the (005) reflection, which has 7 times the intensity of the (002) reflection. Pole figure measurements at the (002) reflection can first allow those specimens to be sorted out which are not eligible for correlations between texture and levitation force of the specimens because of parasitic textures. Figure 5, for instance, shows the (002) pole figure of the M43 specimen with a slight parasitic texture. On the other hand, Fig. 6 shows a clear *c*-axis orientation of the M37 specimen. This pole figure measurement indicates the approximate rotational symmetry of the orientation distribution of *c*-axes around the axis of distribution which differs from the cylinder axis by only 2.5°. The levitation force is relatively high at 87.0 N.

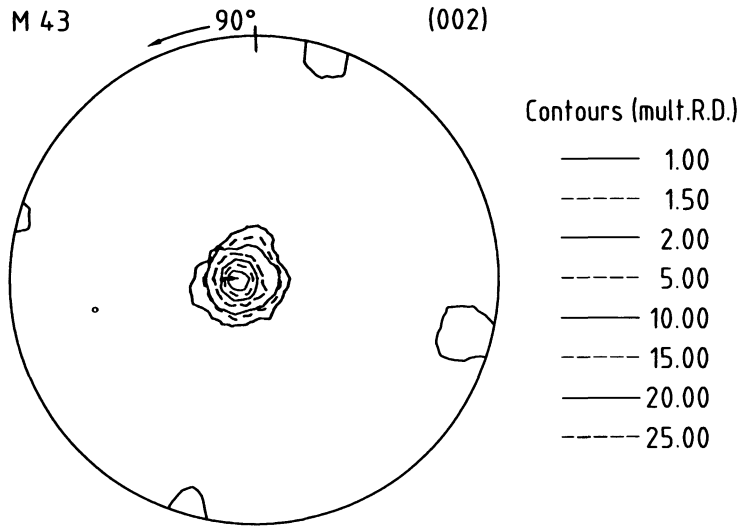

FIGURE 5 (002) pole figure of specimen M43. The distribution axis of *c*-axis distribution is tilted due to the cylinder axis by 7°, a small *a*/*b*-axis orientation in parallel to the cylinder axis is admixed.

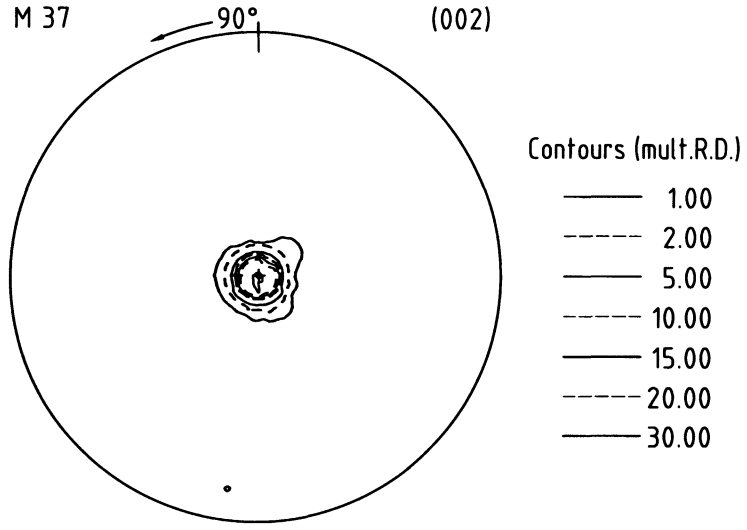

FIGURE 6 (002) pole figure of specimen M37. The distribution axis and the cylinder axis coincide in this measurement (mesh width 6°). No *a*/*b*-axis orientation is admixed.

4 SECTIONS THROUGH THE POLE SPHERE

To find the angular distance, $\Delta\chi$, of the axis of distribution measured from the cylinder axis, a section must be made through the peak of the (005) pole figure in 1° steps in χ. This peak can be found by refining the step width in φ to 10° and even less. If the peak of orientation distribution, e.g., has an angular distance of 6° from the cylinder axis, a step width in φ, of 10° must be used and, at a pole distance of 12° from the axis of distribution, a step width in φ of 5°, so that the step width of 1° and, hence, the same resolution in φ as in χ is achieved on great circles of the pole sphere at the peak of the orientation distribution of the *c*-axes.

If previous pole figure measurements indicate that the distribution of the orientation of *c*-axes is sufficiently rotationally symmetrical, two sections through the pole sphere are sufficient, namely at φ and at $\varphi + \pi$, provided that the peak of orientation distribution has been located precisely at the point φ. The axial deviation of the axis of distribution from the cylinder axis ($\Delta\chi$) can be determined from these two sections, as can be the full-width at half-maximum (FWHM) distribution. The sum total of both quantities ($\Delta\chi$ + FWHM) represents a first approximation to the quality of the texture, provided that the section through the pole sphere is roughly Gaussian, i.e., the distribution has no more or less extended other components. Figure 7 shows a section, not quite

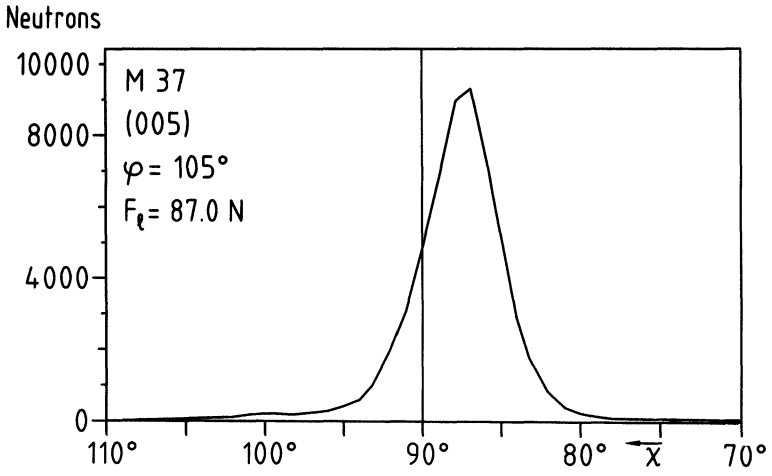

FIGURE 7 Section through the (005) pole sphere of specimen M37. This distribution is not Gaussian formed. The levitation force is smaller than at specimen M39.

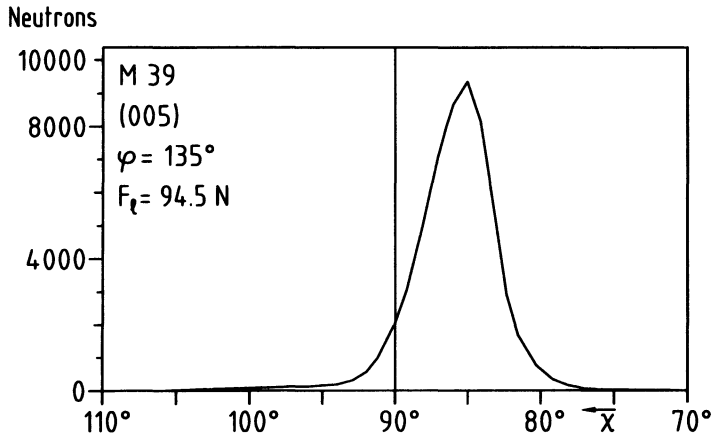

FIGURE 8 Section through the (005) pole sphere of specimen M39. This distribution is well Gaussian formed. The polar distance of the maximum of the distribution is 5°. The levitation force is 94.5 N.

Gaussian, through the (005) pole sphere of the M37 specimen, while the section through the (005) pole sphere of the M39 specimen in Fig. 8 is nearly Gaussian.

Although, in the M39 specimen, the pole distance of the axis of distribution from the cylinder axis is 5°, the M39 specimen has the highest measured levitation force of 94.5 N. The pole distance of the axis of distribution relative to the cylinder axis is only 2.5° in the M37 specimen and as the other components of the distribution are more important on the small circles, which become larger with the pole distance, this M37 specimen attains a levitation force of only 87.0 N, which is 7.5 N less than that achieved by the M39 specimen with the larger pole distance of the distribution axis from the cylinder axis at roughly the same FWHM distribution.

5 NEW DISTRIBUTION OF POLE DISTANCES OF THE *c*-AXES FROM THE CYLINDER AXIS

When the approximate rotational symmetry around the distribution axis can be reasonably assumed on the basis of pole figure measurements, an equal-area measurement with 1° mesh width can be simulated. This saves valuable measuring time. The small circle rings of the pole

figure to be generated by means of the section contain subdivisions in the sequence of 6, 12, 18, etc. Now the respective measured value of the section through the pole sphere is entered into each surface element of a small circle ring, with all surface elements of a small circle ring having the same value. For the 0.5–1.5° interval, the value of 1° distance from the peak *c*-axes orientation distribution applies; for the 1.5–2.5° interval, it is the value of 2° distance from the peak; for the 2.5–3.5° interval, it is 3° distance, etc. For simplicity's sake, the distributions were symmetrized, i.e. the left and the right halves of the distributions were averaged in each case. This is why all surface elements show the same values on the small circle rings around the distribution axis.

Now the rotationally symmetric distribution is cut, as shown in Figs. 9 and 10, also on small circles, but this time about the cylinder axis. All values situated on a small circle ring around the cylinder axis are summed up. Out of the individual sums are produced the values of the distribution of axial deviation of the *c*-axes of the domains relative to the cylinder axis, as can be seen, by a way of example, for the M39 specimen

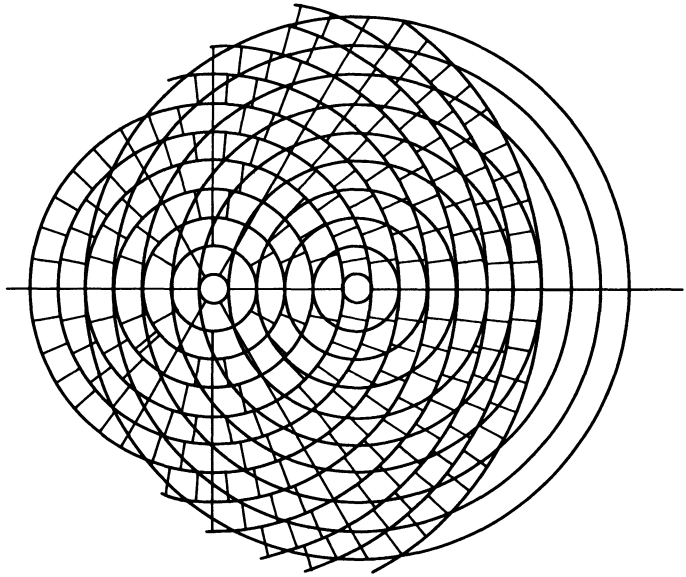

FIGURE 9 Grid for cutting the rotational symmetric distribution on small circles around the cylinder axis. At left hand side cylinder axis, at right hand side axis of distribution.

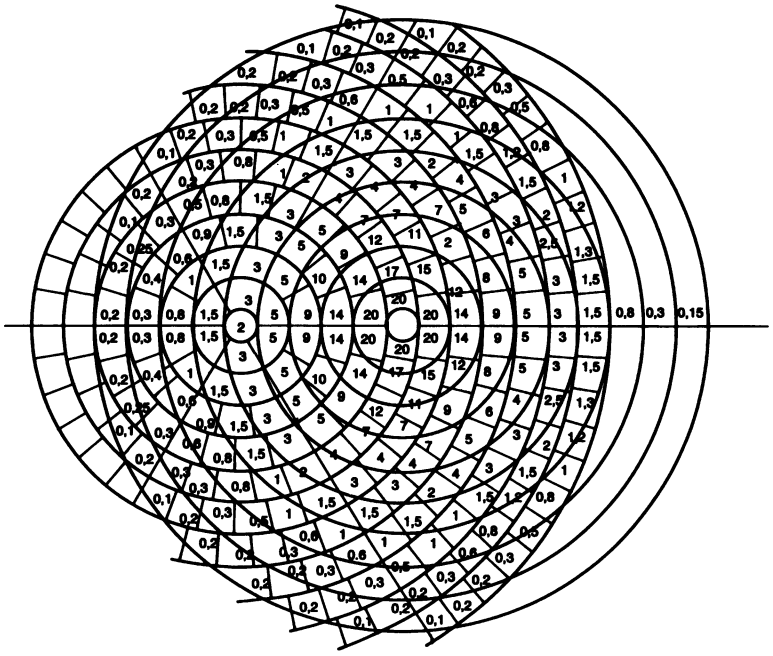

FIGURE 10 In the grid of Fig. 9 on the distribution the values are interpolated. The sums on small circle rings around the cylinder axis represent the values of the distribution of *c*-axis deviations from the cylinder axis.

in Fig. 11. In this new distribution of the M39 specimen, 94% of the axial deviations of the *c*-axes of the domains are below the value of $\Delta\chi +$ FWHM. For the M40 specimen, however, the value of $\Delta\chi +$ FWHM includes only 75.4% of all orientations of the *c*-axes, while 94% of the orientations are below 18° pole distance, see Fig. 12.

6 LEVITATION FORCE–TEXTURE CORRELATION

Plotting the correlation of the levitation force versus the value of $\Delta\chi +$ FWHM produces an erroneous picture (Fig. 13) because the effect of the other components of the distribution and also of a large random fraction is not taken into account in the M43 specimen.

The 94% value of all orientations is a good measure for comparing the levitation forces of specimens. This refers to the pole distance within which 94% of all *c*-axis orientations are located. This situation is shown

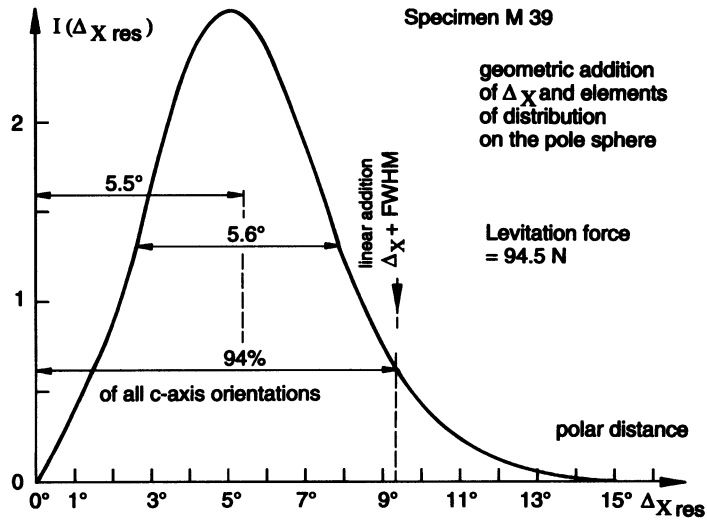

FIGURE 11 Resulting distribution for specimen M39. The limit $\Delta\chi + \text{FWHM}$ includes 94% of all c-axis orientations.

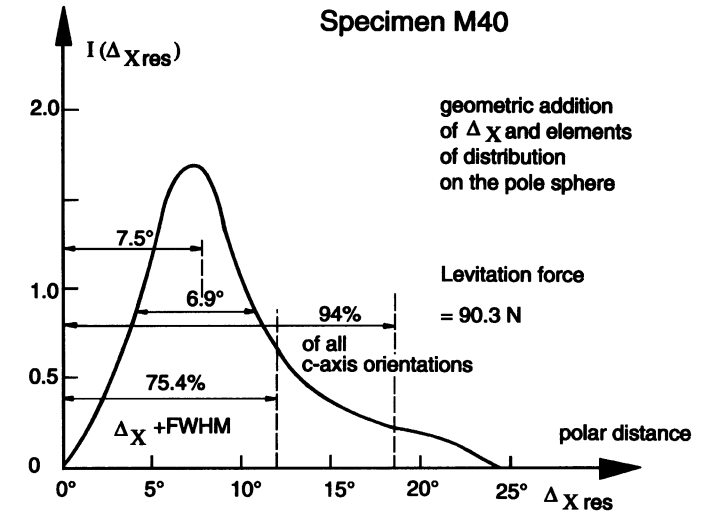

FIGURE 12 Resulting distribution for specimen M40. The limit $\Delta\chi + \text{FWHM}$ includes only 75% of all c-axis orientations.

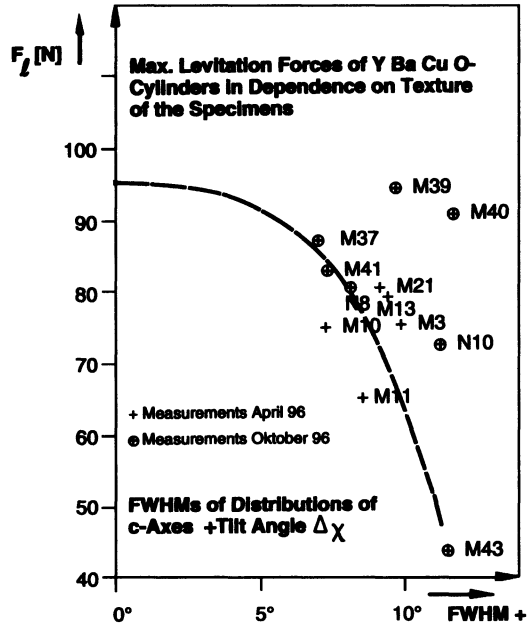

FIGURE 13 False correlation between levitation force of specimens and texture not taking into account the isotropic fraction of specimen M43.

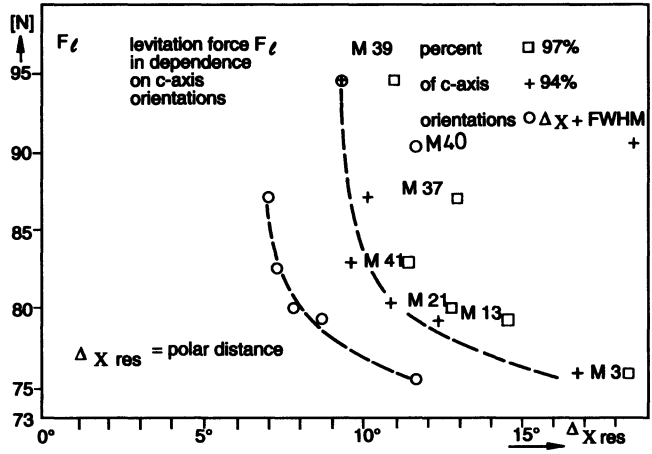

FIGURE 14 Correlation between levitation force of selected specimens (free of microcracks and other orientations). The three values, $\Delta\chi + \text{FWHM}$, 94% limit and 97% limit of orientations are plotted.

in Fig. 14 for seven selected specimens. The M40 specimen is an outlier. It could be that the local textures of the M39 specimen and of the M40 specimen differ considerably and, consequently, despite a high 94% value at an angle of 18°, the M40 specimen has a relatively high levitation force of 90.3 N.

7 COMPARISON OF THE TEXTURES OF THE M43 AND M37 SPECIMENS

Finally, an explanation would be presented of the fact why, despite the absence of a measurement of the isotropic fraction of the M43 specimen, this contains a high random fraction of *c*-axis orientations. Fig. 15 shows

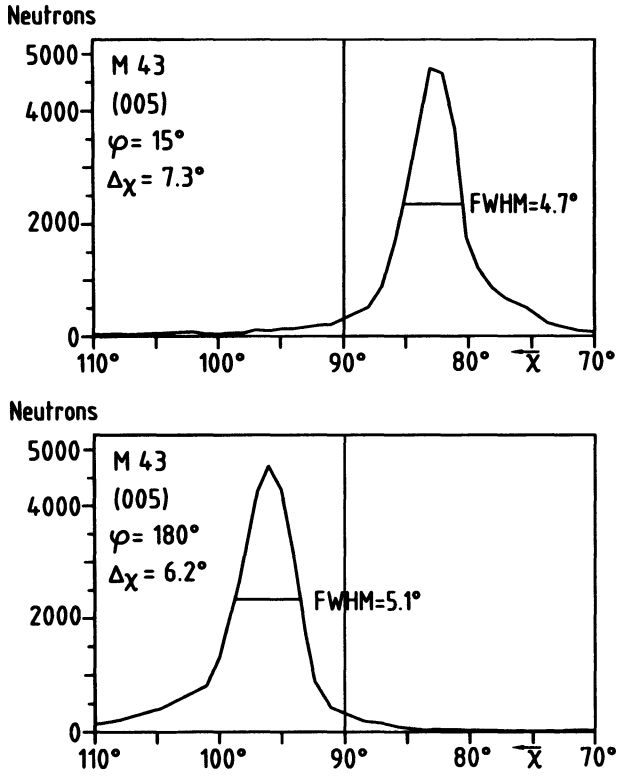

FIGURE 15 Section through the (005) pole sphere meeting the maximum of orientation distribution of specimen M43. Because of an isotropic fraction the counting rate in the maximum is nearly half of that of specimen M37.

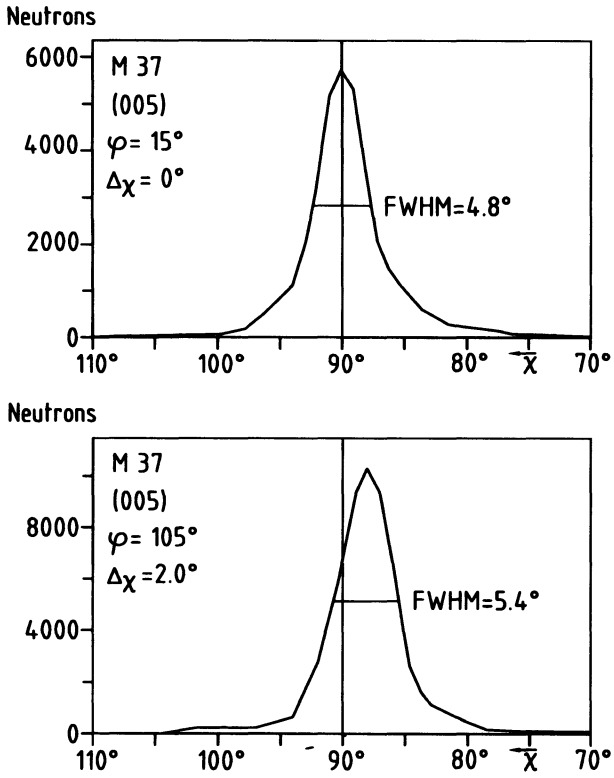

FIGURE 16 Section through the (005) pole sphere, above: not meeting the maximum, and at bottom: meeting the maximum of the distribution. The counting rate in the maximum is nearly twice of that of specimen M43.

the sections through the pole sphere of the M43 specimen. The FWHM sections are similar to those of the M37 specimen (Fig. 16). The counting rates are indicated along the vertical axes of the sections. While in the M43 specimen (Fig. 15) both sections pass through the peak, Fig. 16 for the M37 specimen shows two sections orthogonal to each other through the (005) pole sphere. One section at $\varphi = 105°$ fits the peak distribution at approximately 10,000 counts. The sections through the peak distribution of the M43 specimen show slightly less than 5000 counts at the peak, for the same monitor counting rate. This, i.e., the approximately half as high integral counting rate in the peak for the same monitor counting rate, explains why the M43 specimen has only approximately half the levitation force (43.6 N) than that shown by the M37 specimen with

87.0 N. Consequently, the M43 specimen cannot be used in establishing a correlation between the levitation force and the texture.

8 LOCAL TEXTURE OF SPECIMEN M39

To investigate a possible case of tilting directions of the distribution axes of *c*-axes distributions of individual parts of a YBaCuO cylinder (see Fig. 17) the specimen M39 was cut into 9 pieces, 1 central piece and 8 pieces at the periphery of the specimen, see Fig. 18. The result of the measurement of the local texture shows that the pieces at the periphery in a diagonal direction of the rectangular seed crystal show the largest deviations of the *c*-axes from the cylinder axis. But no evidence of a

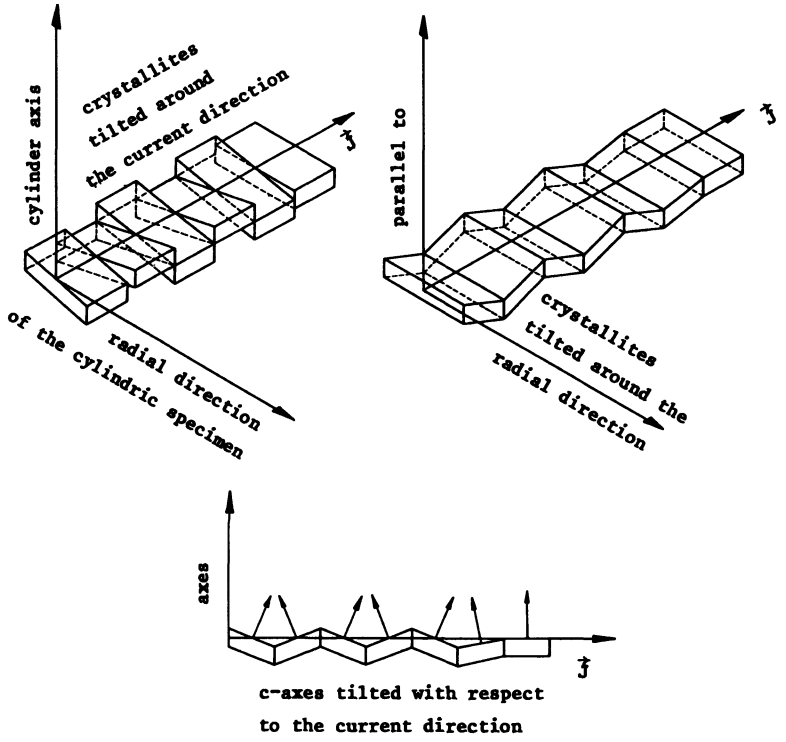

FIGURE 17 Possible orientations of the *c*-axes of crystalline domains. Tilting around the current direction of the induced superconducting current diminishes the current carrying capacity only slightly at a field of 1 T.

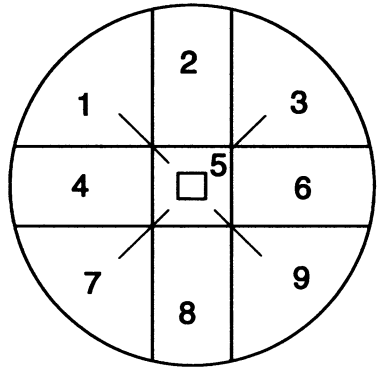

FIGURE 18 To investigate the local texture of specimen M39 this specimen was cut into 9 pieces, 1 central piece with the seed crystal and 8 pieces at the periphery.

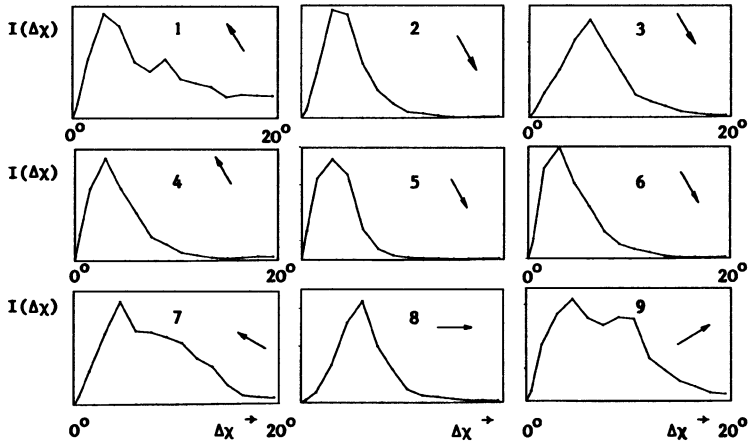

FIGURE 19 Distributions of *c*-axis deviations from the cylinder axis of specimen M39. The arrows indicate the tilting directions of the distribution axes of the 9 pieces. The mesh width of the equal-area measurement was 1.5°.

preferred tilting direction of the distribution axes of the parts each one in the same plane with the cylinder axis was found. The arrows in Fig. 19 indicate the tilting directions of the axes of *c*-axis orientation distributions of the 9 pieces of specimen M39. The (002) pole figures are shown in Fig. 20 (Jung *et al.*, 1997; 1998).

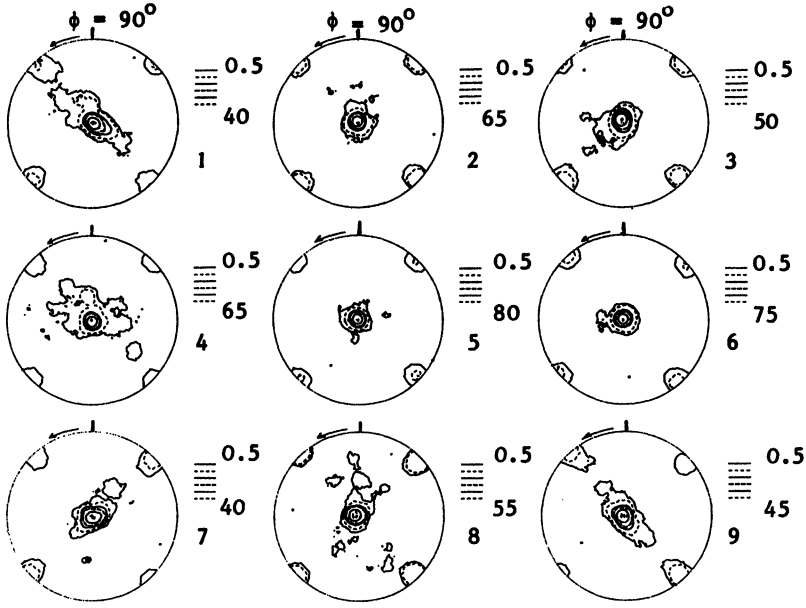

FIGURE 20 (002) pole figures of the 9 pieces of specimen M39. The pole figures are arranged in the same position as the pieces are cut (see Fig. 18). Pieces in diagonal direction of the rectangular seed crystal show the largest deviations of the *c*-axes from the cylinder axis of the YBaCuO cylinder.

References

Bogner, G. (1988) Potential effects of the new high-temperature-superconductors on energy systems. *Proc. 10th Int. Conf. on Magn. Lev. Syst. (Maglev)*, Hamburg pp. 381–390.

Bornemann, H.J., Urban, C., Boegler, P., Küpfer, H. and Rietschel, H. (1993a) Melt-textured Y–Ba–Cu–O and its applications to autostable superconducting magnetic bearings. Advances in Superconductivity-VI, *Proc. of the Int. Symp. on Superconductivity*, October 26–29, Hiroshima, Springer Verlag, Heidelberg, pp. 1311–1316.

Bornemann, H.J., Boegler, P., Urban, C., Zabka, R., Rietschel, H., de Rango, P., Chaud, X., Gautier-Picard, P. and Tunier, R. (1993b) YBaCuO texturation and applications of superconducting magnetic bearings in flywheels for energy storage. *Applied Superconductivity*, Vol. 1, H.C. Freyhardt (Ed.) DGM Informationsgesellschaft Verlag, pp. 277–283.

Bornemann, H.J., Tonoli, A., Ritter, T., Urban, C., Zaitsev, O., Weber, K. and Rietschel, H. (1995) Engineering prototype of a superconducting flywheel for long term energy storage. *Applied Superconductivity Conference 1994*, Boston, USA, *IEEE Transactions on Appl. Supercond.*, Vol. 5, pp. 618–621.

Bornemann, H.J., Brokmeier, H.-G., Burghardt, T., Hennig, W., Jung, V. and Zink, U. (1996) Neutron texture measurement on solid YBaCuO specimens with a view to manufacturing a superconducting magnetic bearing. Textures of Materials,

Proceedings of the Eleventh International Conference on Textures of Materials, Vol. 2, pp. 951–955. ICOTOM 11, Xi'an.

Bornemann, H.J., Burghardt, Th., Hennig, W. and Kaiser, A. (1997) Processing technique for fabrication of advanced YBCO bulk materials for industrial applications. *Applied Superconductivity Conference*, Pittsburgh, PA, USA, August 25–30, 1996, *IEEE Transactions on Applied Superconductivity*, pp. 1805–1808.

Brokmeier, H.-G. (1995) Texturanalyse mittels winkeldispersiver neutronogra-phischer Kernstreuung. GKSS 95/E/9.

Gross, R. (1993) In: *Interfaces in High-T_c Superconducting Systems*, Springer-Verlag, Heidelberg, pp. 176–209.

Jung, V. (1988) *Magnetisches Schweben*, Springer-Verlag, Heidelberg, p. 64.

Jung, V., Adam, M., Bornemann, H.J., Brokmeier, H.-G., Kaiser, A., Schnieber, R. and Thoms, J. (1997) Texture of superconducting YBaCuO-cylinders and their levitation force repulsing an inducting permanent magnet. FZKA 5961, Forschungszentrum Karlsruhe.

Jung, V., Adam, M., Bornemann, H.J., Brokmeier, H.-G., Kaiser, A. and Schnieber, R. (1998) The influence of a seed crystal on the texture of a bulk YBaCuO specimen. FZKA 6072, Forschungszentrum Karlsruhe.

Schochlin, A., Ritter, T. and Bornemann, H.J. (1995) Optimized configurations of autostable superconducting magnetic bearings for practical applications, *IEEE Transactions on Magnetics*, Vol. 31(6), pp. 4217–4219.